THE JOURNAL OF PHYSICAL CHEMISTRY C

Article

pubs.acs.org/JPCC

New Luminescent Host–Guest System Based on an Iridium(III) Complex: Design, Synthesis, and Theoretical–Experimental Spectroscopic Characterization

Thiago B. de Queiroz,[†] Moema B. S. Botelho,[†] Jesús M. Fernández-Hernández,[§] Hellmut Eckert,[†,∥] Rodrigo Q. Albuquerque,[‡] and Andrea S. S. de Camargo*[,†]

[†]Laboratório de Espectroscopia de Materiais Funcionais (LEMAF), Instituto de Física de São Carlos and [‡]Laboratório de Química Supramolecular, Instituto de Química de São Carlos, Universidade de São Paulo, São Carlos, SP, 13566-590, Brazil

[§]Institute of Physics and Center for Nanotechnology and [∥]Institut für Physikalische Chemie, Westfälische Wilhelms-Universität Münster, Münster, 48149, Germany

Supporting Information

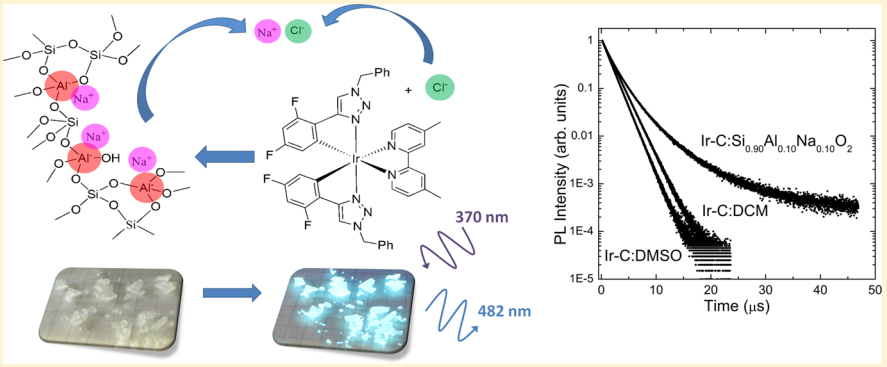

ABSTRACT: This work presents the design, preparation, and characterization of a very efficient solid state luminescent material based on a cationic bis-cyclometalated Ir(III) complex $[Ir(dfptrBn)_2(dmbpy)]^+$ (dfptrBn = 1-benzyl-4-(2,4-difluorophenyl)-1*H*-1,2,3-triazole; dmbpy = 4,4′-dimethyl-2,2′-bipyridine) encapsulated in sodium aluminosilicate mesoporous sol–gel glasses via the ion exchange process. The optical properties of the Ir(III) complex were fully characterized in solution and in the mesoporous solid host. The employed approach resulted in irreversible encapsulation of the complex and superior photophysical properties, such as increased photoluminescence lifetime values. Density functional theory (DFT) and time-dependent DFT (TDDFT) calculations were carried out to understand how the chemical environment around the Ir(III) complex influences its photophysical properties. In particular, we show that in low-polarity media ($\varepsilon < 20$) the coupling between the cationic Ir(III) complex and the counterion appreciably affects its electronic structure.

1. INTRODUCTION

Iridium(III) complexes are among the most studied systems for modern luminescent applications.[1] It is remarkable that these complexes can be tailored to emit over the whole visible spectral range with short emitting lifetimes (of the order of microseconds) and luminescent efficiencies close to unity in deaerated conditions.[2] Such properties make these emitters particularly attractive for electroluminescent applications as highly efficient organic light emitting diodes (OLEDs)[1b,3] or more recently in light-emitting electrochemical cells (LECs).[2c,4] Furthermore, these complexes are interesting candidates for molecular labeling agents and gas sensing,[5] as photosensitizers in solar cells,[6] in electrochemiluminescence (ECL) detection,[7] and in photocatalysis.[8] In many of these applications, the photoactivity of the Ir(III) complex is exploited within a solid host matrix, responsible for promoting molecular dispersion and imparting further functionalities on the final material. An ideal host material must provide a stable solid structure that immobilizes the emitter, limiting the degree of interaction with species capable of deactivating excited states, and preventing molecular aggregation. Furthermore, permanent encapsulation, i.e., the absence of leaking effects in liquid media, is desirable. In general, the physicochemical and photophysical properties of the emitter are strongly influenced by the host medium, such as thermal stability and photostability, excitation and emission spectra, luminescence efficiencies, concentration-quenching rate constants, and host–guest energy transfer rates.[1b,e,4b,8b,9] Some successful approaches for cyclometalated Ir(III) complexes include incorporation into mesoporous silicates,[1e,10] covalent attachment to functionalized organosilica matrices,[8b]

Received: October 5, 2012
Revised: January 12, 2013
Published: January 16, 2013

and blending with copolymers.[1c,9b,11] Although large progress has been achieved since the first solid state luminescent materials based on transition metal complexes were developed,[3,12] many issues still need to be addressed, as complicated synthetic and deposition steps,[1b,2d,11a] difficulties on host−guest exciton matching,[1b,11b,13] and luminescent quenching effects, caused by aggregation and binding of molecular oxygen.[14] Pursuing some of these issues, we recently developed a one-step synthesis to prepare an Ir(III) metallosurfactant complex immobilized in mesoporous silica via a self-assembly mechanism, which has exhibited high quantum yields when compared to the metallosurfactant in solution.[10a] The drawback of this system, however, is the rather complex procedure of synthesizing the metallosurfactant and carrying out the self-assembly reaction. Furthermore, as the Ir(III) complex is not attached to the host, substantial leakage is expected (and observed) upon exposure to liquid media.

In the present contribution we use a simple ion exchange reaction for permanently immobilizing cationic Ir(III) complex within glassy mesoporous sodium aluminosilicate matrices ($Si_{1-x}Al_xNa_xO_2$), prepared by sol−gel methodology.[15] This host network possesses anionic tetrahedral $(AlO_4)^-$ sites that are charge balanced by exchangeable sodium cations. In particular, we report the encapsulation of the bis-cyclometalated cationic Ir(III) complex $[Ir(dfptrBn)_2(dmbpy)]^+$ (dfptrBn = 1-benzyl-4-(2,4-difluorophenyl)-1*H*-1,2,3-triazole; dmbpy = 4,4′-dimethyl-2,2′-bipyridine)[16] into mesoporous glasses with Si/Al ratios of 2, 6, and 9 (a schematic representation of the Ir(III) complex and of the sodium aluminosilicate network are presented in section S1 of the Supporting Information). The Si/Al ratios are varied in an effort to enhance the degree of dispersion of the Ir(III) complex molecules and adjust their medium polarity (dielectric constant). The materials are investigated by steady-state spectroscopy, photoluminescence lifetime measurements, and absolute quantum yield determination. The results are interpreted with the assistance of the density functional theory (DFT) and time-dependent DFT (TDDFT).

Additionally, the DFT and TDDFT calculations were extended to investigate the photophysical properties of the Ir(III) complex influenced by the chemical environment (medium polarity and counterion). Indeed, the description of the electronic structure of the emitter,[1f,2b,17] the host−guest charge transfer,[11b,13] and quenching mechanisms[9a,14] are topics for extensive experimental and theoretical studies. These contributions have been of fundamental importance for the design and optimization of optical devices benefiting from host−guest cooperative effects and synergies. However, when it comes to the description of the electronic structure of Ir(III) complexes in solid hosts, with few exceptions,[1f,11b,18] most studies neglect the chemical environment, such as the polarity of the medium, and more often, the influence of the counterion.[2b,c,19] One of the objectives of this manuscript is to address these issues from a theoretical point of view.

2. EXPERIMENTAL SECTION

2.1. Sample Preparation and Characterization. Mesoporous sodium aluminosilicate glasses with compositions $Si_{0.67}Al_{0.33}Na_{0.33}O_2$, $Si_{0.86}Al_{0.14}Na_{0.14}O_2$, and $Si_{0.90}Al_{0.10}Na_{0.10}O_2$ were prepared according to Deshpande et al.[15] using an aqueous sol−gel route with aluminum lactate ($Al(lact)_3$, 98%, Fluka), tetraethoxysilane (TEOS, 98%, ABCR), and sodium acetate (98%, Fluka) as precursors. In a typical preparation, 1.174 g of $Al(lact)_3$ and 0.328 g of sodium acetate are dissolved in 30 mL of distilled water. Simultaneously, a solution of 1.8, 5.3, and 8.0 mL (8, 24, and 36 mmol) of TEOS (amount of TEOS based on the target composition) in 10 mL of ethanol is stirred for 1 h. The two solutions are mixed and the pH is adjusted to 4.0 with nitric acid (1 M) or ammonia solution (1 M), and controlled within 0.1 units by using a pH meter (WTW pH 320, Germany). After 24 h of stirring, the resultant clear solution is poured into Petri dishes and gelled for 2 weeks at room temperature, which leads to a transparent xerogel. The annealing of the gels is done at 120 °C for 2 days in a Heraeus muffle furnace and subsequently at 650 °C for 5 h with heating and cooling rates of 2 °C/min in a Nabertherm HTC 03/14 furnace.

Prior to the complex incorporation, the network structure of the glasses was confirmed by high resolution solid state NMR of the ^{29}Si, ^{27}Al, and ^{23}Na nuclei. ^{29}Si MAS NMR spectra were recorded on a Bruker CXP-300 spectrometer at a resonance frequency of 59.6 MHz in a 7 mm MAS NMR probe operated at a rotor frequency of 4 kHz, using single pulse excitation with 90° pulses of 6.0 μs length and a recycle delay of 40 s. The ^{29}Si chemical shifts were externally referenced to tetramethylsilane. The Al and Na environments were further characterized by triple quantum (TQ) MAS NMR, which serves to separate the Zeeman interactions from quadrupole interactions and allows determination of isotropic chemical shifts. These experiments were carried out on a Bruker DSX-500 spectrometer using a three-pulse z-filtering method[20] with resonance frequencies of 132.2 and 130.3 MHz for ^{23}Na and ^{27}Al, respectively, and MAS frequencies of 14 kHz. TQ excitation pulse and reconversion pulse lengths for both nuclei were 2.3 and 0.8, respectively, at a ^{27}Al nutation frequency of 120 kHz and ^{23}Na nutation frequency of 115 kHz (liquid standard). The single quantum coherence was detected with a soft pulse (nutation frequency 8 kHz) of 7.6 μs length and 256 t_1 data sets incremented by 4 μs were accumulated in 128 scans. ^{27}Al and ^{23}Na isotropic chemical shifts are reported relative to aqueous solutions of $Al(NO_3)_3$ (1M) and NaCl (1M), respectively.

The ^{27}Al TQ-MAS NMR spectra of $Si_{0.67}Al_{0.33}Na_{0.33}O_2$, $Si_{0.86}Al_{0.14}Na_{0.14}O_2$, and $Si_{0.90}Al_{0.10}Na_{0.10}O_2$ samples (Supporting Information, section S2) are characterized by one peak at the isotropic chemical shift of 64.3, 61.8, and 61.4 ppm, respectively, which is attributed to the anionic tetrahedral AlO_4 unit linked to $Q^{(4)}$ silica. No higher-coordinated aluminum species were detectable. Also, ^{23}Na TQ-MAS NMR spectra (Supporting Information, section S3) present one peak at the isotropic chemical shift of −13, −5.2, and −4.6 ppm for the $Si_{0.67}Al_{0.33}Na_{0.33}O_2$, $Si_{0.86}Al_{0.14}Na_{0.14}O_2$, and $Si_{0.90}Al_{0.10}Na_{0.10}O_2$ samples, respectively. The ^{29}Si MAS NMR data (Supporting Information, section S4) reveal tetrahedral units with centers of gravity near −93.8, −100.5, and −102.5 ppm for the $Si_{0.67}Al_{0.33}Na_{0.33}O_2$, $Si_{0.86}Al_{0.14}Na_{0.14}O_2$, and $Si_{0.90}Al_{0.10}Na_{0.10}O_2$ samples, respectively. The average ^{29}Si chemical shift increases systematically with increasing Al content, reflecting an increase of the average number of Si−O−Al linkages in the second coordination sphere of silicon. These data are in good agreement with previously published data on similar compositions[15,21] and confirm that the expected tetrahedral Si and Al species are formed, with the latter being charge compensated by sodium cations.

The porosities and surface areas of the host matrices were characterized by N_2-sorption measurements at 77 K, using a Micromeritics ASAP 2010 volumetric adsorption analyzer.

dx.doi.org/10.1021/jp309873y | J. Phys. Chem. C 2013, 117, 2966−2975

Before the analyses, 200−300 mg of the samples were outgassed at 120 °C, for at least 12 h under vacuum (≤6 μm Hg). The specific surface area was calculated according to the Brunauer−Emmett−Teller (BET) equation,[22] using nitrogen adsorption data in the relative adsorption range from 0.06 to 0.2. The total pore volume V_p, was obtained from the amount of N_2 adsorbed at p/p_0 of about 0.99. Mesopore size distributions were obtained by applying the Barrett−Joyner−Halenda (BJH) method, assuming a cylindrical pore model.[23]

Bulk densities of the mesoporous matrices were measured by the Archimedes method, according to $\rho_g = (m_D \cdot \rho_{H_2O})/(m_W - m_I)$, where m_D is the weight of the dried sample (at 150 °C), ρ_{H_2O} is the water density, m_W is the weight of the sample after boiled in water (100 °C) for 1 h and superficially dried, and m_I is the weight of the samples immersed in water. The densities are 1.36(1), 1.397(2), and 1.503(2) g/cm^3 for the samples $Si_{0.67}Al_{0.33}Na_{0.33}O_2$, $Si_{0.86}Al_{0.14}Na_{0.14}O_2$, and $Si_{0.90}Al_{0.10}Na_{0.10}O_2$, respectively. Interestingly, for all compositions, the volume occupied by the water in the pores was approximately 0.25 cm^3/g, similar to the pore volume estimated by N_2 sorption (see Results and Discussion below).

The ion exchange intercalation reaction of the Ir(III) complex with the sodium aluminosilicate matrices was done by agitating 300 mg of the host materials in 10 mL of dichloromethane (DCM) solutions of the Ir(III) complex with concentrations 10^{-5}, 10^{-4}, and 5×10^{-4} M. After 48 h of agitation, the supernatant solutions showed no significant presence of the Ir(III) complex, as verified by UV−vis absorption experiments. The solid samples were subjected to Soxhlet extractions in DCM (250 mL) for 2 days. The resulting solutions also presented no detectable Ir(III) complex absorption, suggesting that the proposed ion exchange reaction is quantitative. Therefore, the Ir(III) complex/host molar ratios were calculated from the amount of Ir(III) complex available in the initial solution, assuming quantitative uptake. Subsequent to the washing processes, the samples were dried at 120 °C for 48 h and stored at ambient conditions. The samples after incorporation are labeled as Ir−C:$Si_{1-x}Al_xNa_xO_2$ with x = 0.33, 0.14, and 0.10. It is worth mentioning that for the most concentrated solution (5×10^{-4} M) only 1% of the sodium cations available are exchanged by the Ir(III) complex. To demonstrate the importance of the ion exchange mechanism in driving the loading, and of the $(AlO_4)^-$ sites in trapping the cationic Ir(III) complexes, we incorporated the Ir(III) complex using as host the molecular sieve silica MCM-41.[24] This material presents ordered mesopores of 2.4 nm diameter and high surface area (1150 m^2/g), sufficient to host the Ir(III) complex. Although the MCM-41 has no particularly attractive sites to the Ir(III) complex molecules, after wet impregnation with 5×10^{-4} M solution, the material presented bright green-blue emission characteristic of the Ir(III) complex. This incorporation is a consequence of the favored entropy increase. However, contrary to the situation with sodium aluminosilicate glasses, the complex was completely removed from the MCM-41 host upon Soxhlet extraction (using DCM as solvent), as confirmed by the absence of photoluminescence emission from the Ir(III) complex in this sample.

2.2. Photophysical Characterization. Absorption spectra were measured in a UV−vis spectrophotometer (Hitachi U-2900) at a 10 nm/min scan rate. Luminescence measurements were conducted in a SPEX Fluorolog 3 spectrophotometer (JOBIN-YVON Inc.) equipped with a photomultiplier detector and a 450 W xenon lamp as an excitation source. Emission and excitation spectra were corrected by the spectral response of the detector and the monochromators, and by the spectral intensity distribution of the lamp. The spectra of 10^{-5} M solutions of the Ir(III) complex in DCM and dimethyl sulfoxide (DMSO), as well as the loaded glasses were investigated. The spectra of thick samples (1.5 mm) were measured in a right angle configuration with the sample oriented in specular angle between the excitation beam and detector to minimize inner filter effects. The emission spectra were recorded by exciting the solid samples at the wavelength of 370 nm and the excitation spectra were recorded by monitoring the emissions at 510 nm. The same equipment was used for the excited state lifetime measurements. In this case, a Nano-LED emitting at 405 nm (fwhm <500 ps) was used as the excitation source and the luminescence signals were acquired in the time correlated single photon counting (TCSPC) mode, using a TBX-4X photodetector. Absolute quantum yields (Φ) were measured in a Hamamatsu Photonics system equipped with a CW Xenon light source (150 W), a monochromator, an integrating sphere and a photonic multichannel analyzer model C7473, with excitation at 370 nm. The measurements were done at ambient conditions (25 °C) but lifetimes were further measured in sealed cuvettes evacuated to 10^{-6} mbar for 24 h.

2.3. Computational Methods. The ground state (S_0) geometry optimization and electronic structure of the Ir(III) complex were obtained by DFT and TDDFT calculations, with the Becke-Lee−Yang−Parr (B3LYP)[25] and Perdew−Burke−Ernzerhof−Adamo (PBE0)[26] functionals. The geometry optimization was performed with unconstrained symmetry, using as initial geometry trial input data the crystallographic structure known from X-ray diffractometry (XRD).[16] The calculations were performed without counterion and with the chloride as counterion, in vacuum or in different dielectric media through the polarized continuum model (PCM).[27] In the DFT geometry optimization, the initial guess for the location of the counterion was based on either the crystal structure[16] or on the molecular electrostatic (MEC) surface, of where the highest accumulation of positive charge is found. Both methods resulted in similar counterion locations, close to the dmbpy ligand, which is in accordance with published data of Ir(III) complexes with similar ligands.[28] Because both methods produced identical results concerning the electronic structure of the Ir(III) complex, all the DFT and TDDFT calculations presented in the following were obtained using the crystallographic structure of the complex as initial guess. The LANL2DZ basis set[29] was employed for the Ir, the 6-31++G basis set[30] for the Cl- and the 6-31G**[31] basis set for additional atoms. The absence of negative vibrational frequencies was confirmed for all optimized structures to further check the reliability of the optimization. The optimized geometries obtained for all calculations were in a good match to the reported crystal structure,[16] as illustrated in the Supporting Information (section S5). TDDFT calculations were carried out using the optimized ground state structures. Calculations of the lowest 120 singlet and triplet excited states allowed us to simulate the absorption spectra down to 220 nm. The simulation of the absorption spectra has been performed by a Gaussian convolution with fwhm = 0.2 eV. Compared to the B3LYP, the PBE0 functional presented the best matching between experimental and calculated data, as illustrated on section S6 of the Supporting Information. It is worth noting that these calculations neglect intersystem crossing processes

dx.doi.org/10.1021/jp309873y | J. Phys. Chem. C 2013, 117, 2966−2975

mixing states of singlet and triplet manifold. For all calculations a Gaussian 09 package was used. The density of states of the specific moieties was acquired with the help of the Gausssum 2.2 program.[32]

Aiming at the closest approximation to the solid matrices, the $[Al(OH)_4]^-$ unit was used as a counterion in these calculations. This unit represents the anionic site of the aluminosilicate matrix, whose charge compensates the positively charged Ir(III) complex in its encapsulated form. These DFT and TDDFT calculations were performed as previously described, with the 6-31++G basis set being used for Al, and including the dielectric constant (ε) of the different matrices via the PCM method.[27] The experimental ε values of the $Si_{0.90}Al_{0.10}Na_{0.10}O_2$ and $Si_{0.86}Al_{0.14}Na_{0.14}O_2$ samples are 15.6 and 18.4, respectively. These values were determined by impedance spectroscopy, from room temperature (25 °C) to approximately 400 °C, in steps of 30 °C, using the experimental setup and procedures described elsewhere.[33] Unfortunately, measurements of the dielectric constant of the composition $Si_{0.67}Al_{0.33}Na_{0.33}O_2$ could not be done due to compromised bulk properties. Overall, calculations of optimized ground state geometries and excited states of the Ir(III) complex were performed without counterion, and with Cl^- or $[Al(OH)_4]^-$ as counterions, in vacuum (ε = 1), DCM (ε = 8.9), $Si_{0.90}Al_{0.10}Na_{0.10}O_2$ (ε = 15.6), $Si_{0.86}Al_{0.14}Na_{0.14}O_2$ (ε = 18.4), DMSO (ε = 46.8), and water (ε = 78.4).

3. RESULTS AND DISCUSSION

Figure 1 illustrates the N_2 sorption−desorption isotherms of the matrices prior to Ir(III) complex incorporation. The

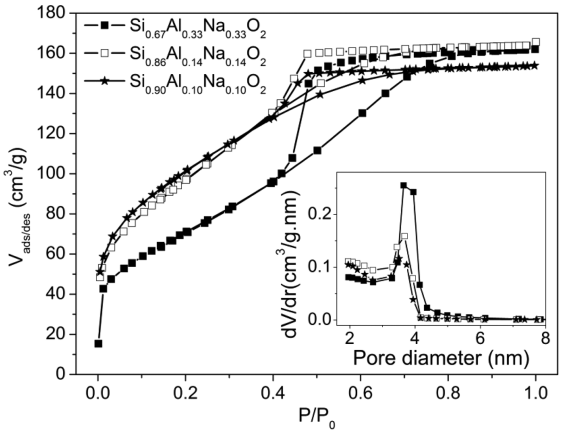

Figure 1. Sorption−desorption isotherms of the sodium aluminosilicate glasses (prior to Ir(III) complex loading). The inset presents the pore size (diameter) distributions of these matrices calculated via BJH algorithm.[23]

matrices present isotherms of type IV with hysteresis loop H2,[34] indicating a mesoporous structure with BET[22] surface areas of 260, 356, and 370 m^2/g, for the $Si_{0.67}Al_{0.33}Na_{0.33}O_2$, $Si_{0.86}Al_{0.14}Na_{0.14}O_2$, and $Si_{0.90}Al_{0.10}Na_{0.10}O_2$ samples, respectively. The inset of Figure 1 presents BJH[23] porous diameter distributions centered at 3.8 nm for all compositions, but with slightly higher microporosity character (ϕ < 2 nm) for the samples with the higher silica contents (Si/Al = 6 and 9). Considering that the approximate diameter of the Ir(III) complex is 1.8 nm, as given by the DFT optimized geometries, we stress that the pores of the matrices are of sufficient size to house one or more complex molecules per pore. Furthermore,

Table 1. Experimental Molar Densities, Emission Maxima, Excited State Lifetimes, and Absolute Quantum Yields of the Encapsulated Ir(III) Complex, and of 10^{-5} M DCM and DMSO Solutions

matrix	[Ir(III) complex][a] (mol/dm^3)	λ_{ems} (nm)	τ_{av}[b] (μs)	Φ[c]
$Si_{0.67}Al_{0.33}Na_{0.33}O_2$	4.6×10^{-4}	482	2.11	0.13
	4.6×10^{-3}	482	1.99	0.17
	2.3×10^{-2}	482	2.13	0.16
$Si_{0.86}Al_{0.14}Na_{0.14}O_2$	4.6×10^{-4}	482	2.04	0.14
	4.6×10^{-3}	482	2.20	0.22
	2.3×10^{-2}	482	1.92	0.19
$Si_{0.90}Al_{0.10}Na_{0.10}O_2$	5×10^{-4}	482	2.03	0.10
	5×10^{-3}	482	2.16	0.16
	2.5×10^{-2}	482	2.63	0.21
DCM	1×10^{-5}	490	1.46	0.21 (0.85)
DMSO	1×10^{-5}	500	1.27	0.22 (0.85)

[a]Based on the amount of Ir(III) complex available in the solution assuming a quantitative ion-exchange reaction. [b]Measured in deaerated conditions (10^{-6} mbar). Section S8 of the Supporting Information provides the multiexponential fitting components of the solid samples. [c]Measurements in deaerated conditions in parentheses. Solid samples could not be measured in such conditions.

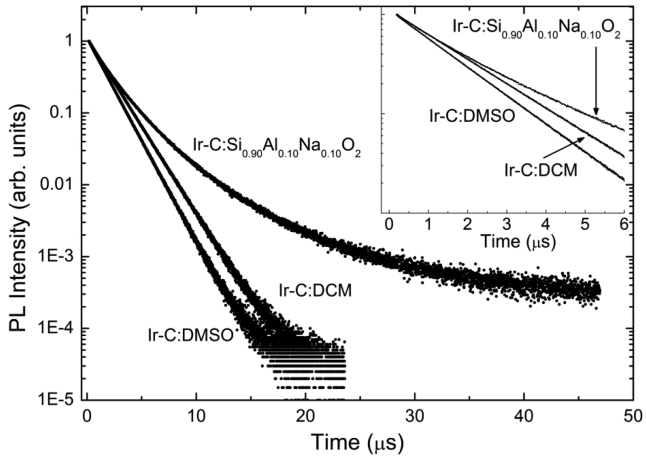

Figure 2. Room temperature photoluminescence lifetime of the Ir(III) complex in 10^{-5} M DCM and DMSO solutions, and in $Si_{0.90}Al_{0.10}Na_{0.10}O_2$ in vacuum (10^{-6} mbar) with excitation wavelength of 405 nm. The inset represents the observation window (up to 6 μs), during which an approximately monoexponential decay is observed in the solid sample.

scanning electron microscope images confirm the homogeneous distribution of pores on the surface of the hosting materials (section S7 of the Supporting Information).

The total volume of pores with diameter between 2 and 4 nm for all samples is higher than 0.2 cm^3/g. Considering a quantitative ion exchange reaction and approximating the Ir(III) complex molecules as spheres of 1.8 nm diameter, we can compare the volume occupied by the incorporated molecules with the total volume of the empty pores in the hosts. The total molecular volume of Ir(III) complexes, contained in 10 mL of the most concentrated precursor solution (5×10^{-4} M), is 9.2×10^{-3} cm^3. Because 300 mg of the host corresponds to at least 6×10^{-2} cm^3 pore volume, this represents an occupancy by the Ir(III) complex of approximately 15% of the total pores available in the hosts. Such loading represents an Ir(III) complex density as high as 2.5 ×

dx.doi.org/10.1021/jp309873y | J. Phys. Chem. C 2013, 117, 2966−2975

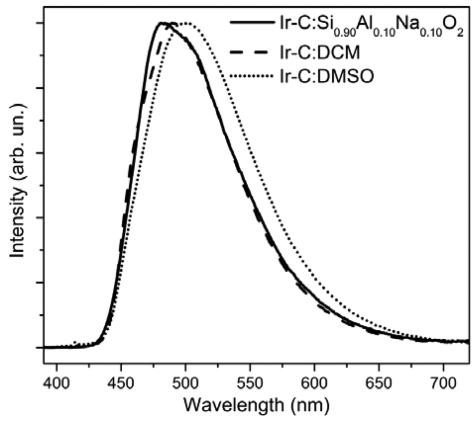

Figure 3. Room temperature emission spectra of the Ir(III) complex in the $Si_{0.90}Al_{0.10}Na_{0.10}O_2$ matrix, in DCM, and in DMSO (10^{-5} M solutions) with an excitation wavelength of 370 nm.

10^{-2} mol/dm^3 in the hosts (Table 1), and considering a homogeneous molecular spatial distribution, an average distance of 4.0 nm between neighboring complex molecules. This distance is higher than the Förster radius for similar Ir(III) complexes dispersed in polymers ($R_0 \leq 2$ nm).[9a] It means that the most concentrated samples have a quantity of emitters in the range at which the photoluminescence decay should not be affected by concentration quenching if the complexes are uniformly dispersed.[9a] Table 1 summarizes the average photoluminescence (PL) lifetime of the samples measured in deaerated conditions, as well as other spectroscopic features. All the host compositions show identical average PL lifetimes, within experimental error, and they are independent of complex concentration within the studied range. Thus, even the most concentrated samples present a negligible portion of Ir(III) complex aggregation within the pores, approaching a homogeneous molecular dispersion.[11b,35]

The average PL lifetimes of the solids ($\tau \sim 2.1$ μs) are significantly longer than the values observed for Ir(III) complex in 10^{-5} M DCM and DMSO solutions ($\tau \sim 1.5$ μs). Figure 2 details the PL decays of a representative sample (Ir–C:$Si_{0.90}Al_{0.10}Na_{0.10}O_2$, 2.5×10^{-2} mol/dm^3), and 10^{-5} M DCM and DMSO solutions. Although the luminescence intensity of the Ir(III) complex in the solutions decays monoexponentially, a more complex behavior is observed in the solid matrix. Within an initial range of ~6 μs, an approximately monoexponential decay characterized by τ = 1.73 μs is observed, which is still longer than the lifetimes in solutions. This increase in the lifetime indicates a decrease of excited state deactivating pathways in the solids compared to the solutions and the absence of energy migration to quenching species distributed in the hosts.[11b,28,36] At longer times, a long tailing is observed, suggesting a large degree of heterogeneity, presumably caused by the disordered environmental character of the sites occupied by the Ir(III) complexes.

Regarding the absolute emission quantum yield (Φ) values, the samples with the highest contents of Ir(III) complex present the best results (up to 22%, in air equilibrated conditions), with the samples of lower Ir(III) complex contents presenting lower Φ values (Table 1). The photoluminescence performance of the Ir(III) complexes in the solid state are frequently reduced by aggregation processes and/or by the relatively low optical quality of the solid hosts compared to the solvents.[1e,2c,d,10,14] The latter issue is the reason for the decrease in Φ values for the samples with the lower contents of Ir(III) complex, similarly to other Ir(III) based host–guest systems.[10] However, the samples with the highest concentration present Φ values comparable to the complex in solution, demonstrating that at such high loadings the absorption of light due to the matrix is irrelevant in comparison with the complex, and that self-quenching effects due to aggregation processes are negligible, as consistent with the lifetime results.

With respect to the general photophysical properties of the Ir(III) complex, there are no noticeable differences among the diverse solid hosts (section S9 and Table 1). Thus the variation of the dielectric medium from 18.4 to 15.6, over the matrix composition range studied, does not seem to considerably affect the electronic structure of the Ir(III) complex. Indeed, our DFT and TDDFT results discussed below show that small differences in the dielectric constants, as observed here, should not considerably affect the energy and composition of the excited states of the Ir(III) complex. For this reason, we will focus the discussion on the spectroscopic features of the Ir–C:$Si_{0.90}Al_{0.10}Na_{0.10}O_2$ sample containing the highest content of

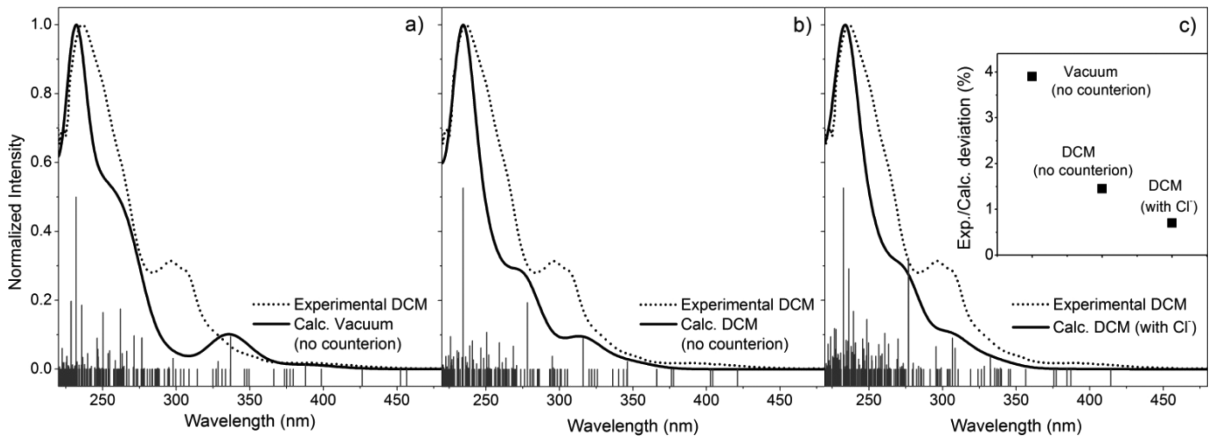

Figure 4. UV–vis absorption spectra of the Ir(III) chloride complex in DCM compared with TDDFT calculated spectra in vacuum (a) in DCM without counterion (b), and in DCM including the counterion (c). Gray bars represent singlet-to-singlet and triplet-to-singlet transitions. The inset of Figure 4c presents the error in the prediction of the excited states, see text. For comparison, experimental and calculated spectra have been rescaled.

dx.doi.org/10.1021/jp309873y | J. Phys. Chem. C 2013, 117, 2966–2975

Table 2. TDDFT Calculated Vertical Transitions under Different Conditions[a]

medium/ counterion	excited state	λ (nm)	f_{osc} [b]	composition[c] (%)	charge transfer (%) Ir	N^N	C^N	C^N′ [d]
Vacuum/No counterion	T_1	457		H → L (96%)	29 → 2	1 → 98	35 → 0	35 → 0
	S_2	452	1×10^{-4}	H → L (97%)	29 → 2	1 → 98	35 → 0	35 → 0
	T_2	426		H−10 → L (42%), H−4 → L (28%)	19 → 3	59 → 97	11 → 0	11 → 0
	S_6	328	0.0181	H−3 → L (64%), H−5 → L (30%)	17 → 3	3 → 97	40 → 0	40 → 0
	S_9	298	0.0254	H → L+3 (90%)	29 → 8	1 → 2	35 → 45	35 → 45
	S_{51}	232	0.3991	H−1 → L+6 (15%), H−5 → L+4 (11%), H → L+15 (11%)	23 → 19	5 → 9	36 → 36	36 → 36
DCM/No counterion	T_1	421		H−10 → L (40%), H−3 → L (24%), H → L (10%)	19 → 2	53 → 95	14 → 2	14 → 1
	T_2	404		H → L (87%)	29 → 3	9 → 97	31 → 0	31 → 0
	S_1	402	2×10^{-4}	H → L (97%)	32 → 3	2 → 97	33 → 0	33 → 0
	S_5	316	0.1112	H−4 → L (75%), H−5 → L (14%)	30 → 2	8 → 97	31 → 0	31 → 1
	S_8	295	0.0477	H → L+3 (88%)	32 → 8	2 → 6	33 → 43	33 → 43
	S_{42}	234	0.6545	H−4 → L+4 (22%), H → L+8 (16%), H−2 → L+5 (15%), H−1 → L+6 (14%)	25 → 6	7 → 8	34 → 43	34 → 43
DCM/Cl^-	T_1	414		H−11 → L (31%), H−6 → L (21%), H−12 → L (13%)	16 → 3	38 → 94	33 → 2	13 → 1
	T_2	387		H → L (91%)	31 → 2	3 → 96	30 → 1	36 → 1
	S_1	384	1×10^{-3}	H → L (97%)	32 → 3	2 → 97	29 → 0	37 → 0
	S_7	308	0.039	H−7 → L (48%), H−6 → L (21%), H−5 → L (21%)	38 → 2	9 → 97	26 → 0	27 → 1
	S_8	307	0.0573	H−7 → L (35%), H−6 → L (37%), H−5 → L (17%)	39 → 1	10 → 97	26 → 1	25 → 1
	S_{10}	295	0.0418	H → L+3 (56%), H → L+2 (21%)	32 → 5	2 → 38	28 → 47	38 → 10
	S_{53}	236	0.1851	H−8 → L+1 (14%), H−6 → L+4 (14%)	27 → 7	9 → 26	30 → 38	34 → 29
	S_{61}	233	0.3338	H−4 → L+6 (36%), H−7 → L+4 (12%)	19 → 6	5 → 5	28 → 26	48 → 63

[a]Transitions are separated in regions of low (460 > λ > 330 nm), intermediate (330 > λ > 280 nm), and high energy (280 > λ > 225 nm). [b]The oscillator strength (f_{osc}) is directly linked to the molecular extinction coefficient. Oscillator strengths of triplet states are not estimated. [c]The HOMO and LUMO are represented by H and L, respectively. [d]C^N′ represents the phenyltriazole ligand placed closest to the counterion.

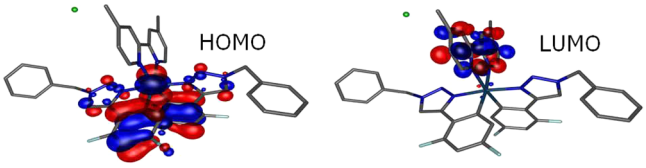

Figure 5. Schematic representation of the electron distribution of the HOMO and LUMO for the Ir(III) chloride complex in DCM (ε = 8.9).

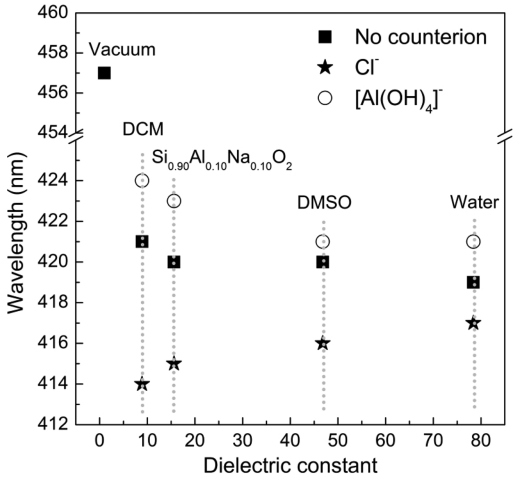

Figure 6. TDDFT calculated $S_0 \rightarrow T_1$ transitions as a function of the dielectric constants without and with Cl^- and $[Al(OH)_4]^-$ as counterions. Above each symbol is indicated the medium that possesses this dielectric constant.

the Ir(III) complex (2.5×10^{-2} mol/dm^3) in comparison with the results in solution (DCM and DMSO, 10^{-5} M).

The emission spectrum at room temperature of the Ir(III) complex in DCM (Figure 3) shows an unstructured band with a maximum at 490 nm, typical for Ir(III) complexes containing a combination of cyclometalated (C^N) ligands and neutral diimine ligands (N^N).[16,28,36a−c] The Ir(III) complex in DMSO (ε = 46.7) presents a red-shifted emission by 400 cm^{-1} in comparison with the complex in DCM (ε = 9.1). This can be attributed to the stabilization of the lowest triplet excited state exerted by environments of higher polarity and indicates that the emitting states have a strong charge transfer (CT) character.[1f] In contrast, the emission spectrum of the Ir(III) complex in the solid matrix (Ir−C:$Si_{0.90}Al_{0.10}Na_{0.10}O_2$, with dielectric constant ε = 15.6), shows a blue shift of about 430 cm^{-1} relative to that in DCM. Furthermore, the emission spectrum of the complex incorporated in the matrix is slightly more structured than in the solutions (DCM or DMSO), with the appearance of a shoulder at approximately 500 nm. These features give clear evidence of the more motion-constrained character of the Ir(III) complex in the solid host (rigidochromic effect).[36d]

The UV−vis absorption of the Ir(III) complex in 10^{-5} M DCM solution is compared with the TDDFT calculations simulating the Ir(III) complex in vacuum (Figure 4a) and in DCM (ε = 8.9), neglecting the counterion (Figure 4b), and in

dx.doi.org/10.1021/jp309873y | J. Phys. Chem. C 2013, 117, 2966−2975

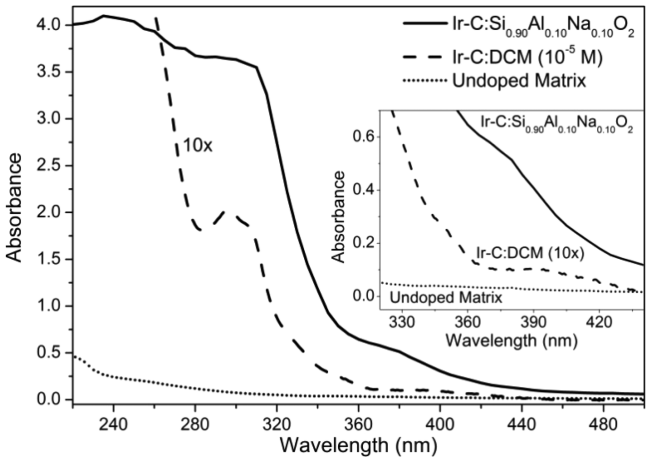

Figure 7. UV−vis absorbance of the Ir(III) complex in $Si_{0.90}Al_{0.10}Na_{0.10}O_2$ and in DCM (10^{-5} M), and of the undoped matrix. The absorbance of the Ir(III) complex in DCM was scaled by a factor of 10. Absorption data of the Ir-C:$Si_{0.90}Al_{0.10}Na_{0.10}O_2$ sample below 330 nm is not reliable due to the complete absorption of the incident light.

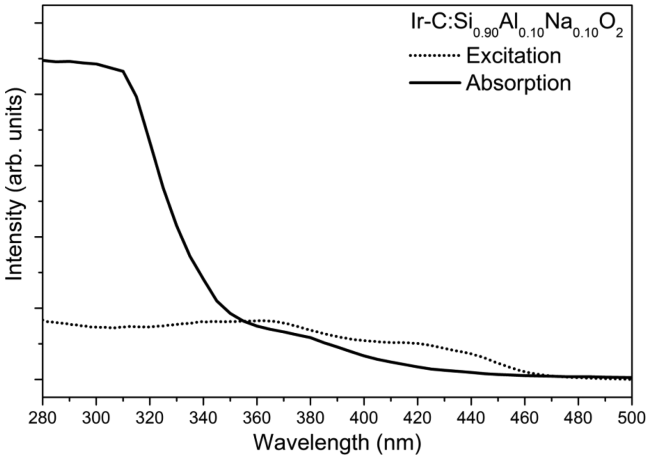

Figure 8. Absorption and excitation (monitored at 510 nm) spectra of the Ir(III) complex in $Si_{0.90}Al_{0.10}Na_{0.10}O_2$. The excitation spectrum is scaled to facilitate the comparison with the absorption spectrum at low energies (λ > 360 nm).

DCM with Cl^- as counterion (Figure 4c). The absorption spectrum of the Ir(III) complex in DCM at room temperature is composed of several broad bands between 220 and 440 nm. The most characteristic transitions are represented by the peaks at an intermediate region, at 309 and 297 nm, and its maximum absorption band at 235 nm, with molar extinction coefficients of 1.7, 1.9, and 6.1 × 10^4 M^{-1} cm^{-1}, respectively.[16] As illustrated by Figure 4a, it is difficult to correlate the experimental peaks at 309 and 297 nm to the transitions calculated in vacuum without the counterion. Indeed, TDDFT calculations tend to overestimate the charge separation upon excitation, which can be diminished by the electrostatic field of the solvent.[37] As shown in Figure 4b, a much better agreement with the experimental spectrum is observed when the dielectric medium is included in the calculations. To quantify the degree of correspondence, we calculated the quantity $\sigma = [\Sigma_1^n(1/n)[(\lambda_i^{exp} - \lambda_i^{calc})/\lambda_i^{exp}]^2]^{1/2}\cdot 100\%$, where n is the number of considered transitions, and λ_i^{exp} and λ_i^{calc} are the wavelengths of experimental and calculated transitions, respectively. As indicated in the inset of Figure 4c, σ decreases from 3.9% to 1.5% when the dielectric medium is taken into account. An even better match (0.7%), especially in the intermediate and low energy regions (λ > 280 nm), is further obtained when including the Cl^- counterion in the calculations. Still, all the calculations, including the one in Figure 4c, show a deficit in intensity when representing the absorption bands in the low and intermediate energy ranges. This is expected as these lower-energy bands contain stronger contributions from singlet/triplet mixed transitions, which are not included in the present TDDFT calculations.

The main features of few lowest energy excited states and the excited states that best characterize the experimental absorption bands simulated using different conditions are listed in Table 2. Most noticeable, in going from vacuum to DCM or DCM with counterion, the calculations indicate an appreciable change in the composition of the lowest excited triplet state (T_1). While in vacuum the $S_0 \rightarrow T_1$ transition is mainly represented by a transition from the highest occupied molecular orbital (HOMO) to the lowest unoccupied molecular orbital (LUMO), in DCM with Cl^- counterion the HOMO → LUMO transition is, in importance, far beneath the H−11 → LUMO (31%), H−6 → LUMO (21%), and H−12 → LUMO (13%) transitions. In addition, the calculation in vacuum presents T_1 with higher charge transfer character than those with the medium included. Accordingly, the calculations performed without considering the chemical environment usually overestimate the ligand-to-ligand charge transfer (LLCT) and metal-to-ligand charge transfer (MLCT) character of the lowest excited triplet state.[37] This result has critical consequences on estimations of radiative transition rates.[38]

Owing to the low resolution of the UV−vis absorption spectrum of the Ir(III) complex in DCM, the transitions calculated with DCM/Cl^- listed in Table 2 are compared with experimental data in blocks of high (280 > λ > 225 nm), intermediate (330 > λ > 280 nm), and low (460 > λ > 330 nm) energies. The complete list of the excited states and their features calculated with DCM/Cl conditions are presented in Table S10 of the Supporting Information. The most intense experimental band (ε > 10^4 M^{-1} cm^{-1}), in the high energy range, has a major contribution from $\pi-\pi^*$ ligand-centered (LC) spin allowed transitions localized on the coordination ligands. At intermediate and lower energy ranges, the transitions have spin-allowed and spin-forbidden character.[16] The intermediate band is mostly composed of spin-allowed LC transitions localized on the ligands and spin-allowed LLCT and MLCT transitions. The band in the lowest energy range is mainly characterized by spin-forbidden transitions[16] and has important contributions from the HOMO → LUMO transition. For instance, the three excited states of lowest energy are mainly accessed by this transition (Table 2). Figure 5 illustrates the optimized molecular structure of the Ir(III) chloride complex in DCM with the electron densities of the HOMO and LUMO. While the HOMO is delocalized over the two phenyl-triazole (C^N) ligands and contains an important contribution on the Ir(III) center, the LUMO is predominantly localized on the diimine ligand (N^N). These features evidence the character of MLCT and LLCT of the HOMO → LUMO transition, and consequently of the band at low energy range.

Given the significance of the counterion in correctly understanding the excited states of the Ir(III) complex, we evaluated the influence of the counterion in different solvents. Figure 6 shows the wavelength of the vertical transition $S_0 \rightarrow$

dx.doi.org/10.1021/jp309873y | J. Phys. Chem. C 2013, 117, 2966−2975

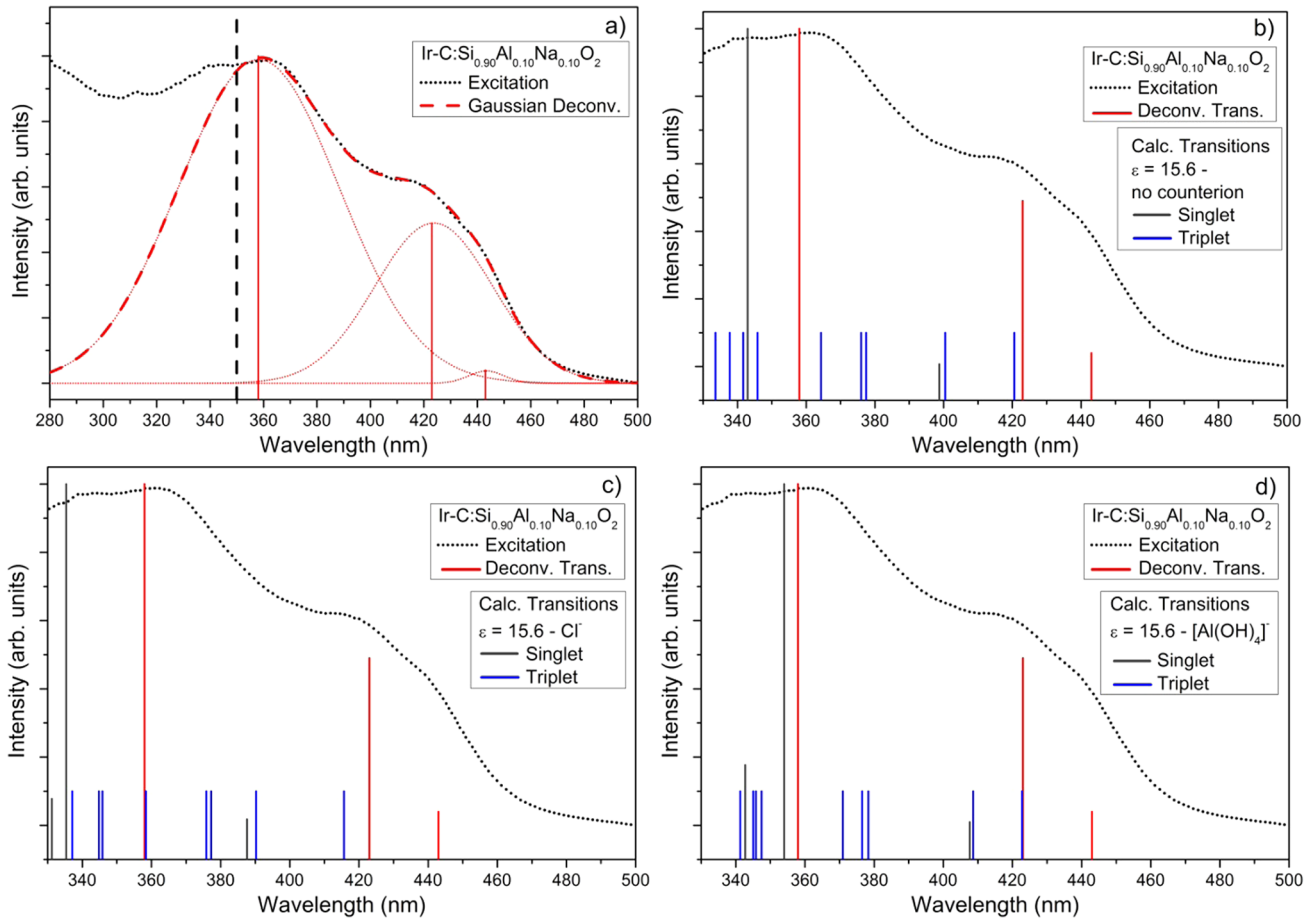

Figure 9. (a) Excitation spectrum (monitored emission at 510 nm) of the Ir(III) complex in $Si_{0.90}Al_{0.10}Na_{0.10}O_2$ and its deconvolution in 3 Gaussians. (b) Comparison with TDDFT transitions calculated in a dielectric medium of ε = 15.6 without counterion, (c) with Cl^- counterion, and (d) with $[Al(OH)_4]^-$ as counterion, considering only transitions with λ > 330 nm. Red bars indicate the experimental transitions, black bars indicate the calculated singlet transitions, and blue bars the triplet transitions. Bars representing the triplet transitions are scaled to a fixed intensity of 0.1. The dashed line crossing the spectrum (a), at 350 nm, separates bands consistent with diffuse excitons (left) from bands predominately formed by confined excitons (right).

T_1 of the Ir(III) complex calculated as a function of the dielectric constant and the counterion. Aside from the result obtained in vacuum, the calculations without counterion predict negligible solvatochromism, presenting a minimal blue shift when the polarity of the medium increases. More considerably, solvatochromism effects are observed when the counterion is included, with Cl^- red-shifting the $S_0 \rightarrow T_1$ transition and $[Al(OH)_4]^-$ blue-shifting it. The effects of the counterions become less pronounced at higher dielectric constants, suggesting that in the limit of high polarities the local charge compensation of the cationic complex is mainly performed by the medium. Comparing the experimental absorption spectra of the Ir(III) chloride complex in DCM (ε = 8.9) and DMSO (ε = 46.8), a small red shift is observed for the latter, with the two characteristic bands in the intermediate energy range (330 > λ > 280 nm) going from 309 and 297 nm to 312 and 299 nm (also illustrated in section S11), which is in accordance with the TDDFT predictions.

UV−vis absorbances of the Ir(III) complex in DCM (10^{-5} M), in the matrix $Si_{0.90}Al_{0.10}Na_{0.10}O_2$ (2.5×10^{-2} mol/dm^3), and of the pure host are shown in Figure 7. The solid samples have similar thicknesses (about 1.5 mm). Aside from the slight differences, the absorbance of the Ir(III) complex in the solid matrix resembles that of the DCM solution down to λ = 330 nm. At shorter wavelengths the solid sample containing the highest concentration of Ir(III) complex (2.5×10^{-2} mol/dm^3) strongly absorbs the incident light, whereas the spectra of the lower concentrated samples are significantly affected by the matrix absorption, particularly above 300 nm (section S12 of the Supporting Information), which complicates their interpretation. More information is accessible from the excitation spectrum, which reflects only the transitions that cause the population of the emitting states. Figure 8 compares the excitation spectrum of the $Ir-C:Si_{0.90}Al_{0.10}Na_{0.10}O_2$ scaled in intensity with the absorption spectrum at longer wavelengths (λ > 360 nm). While the absorbance drastically increases below 350 nm the excitation spectrum changes only gradually, characterizing a region of partial excitation cutoff. The cutoff wavelength ($\lambda \approx$ 350 nm) lies only slightly below the emission maxima of silica xerogels (370 nm) in the presence of organic impurities.[39] These observations suggest that below 350 nm (3.54 eV) the excited states are deactivated by quenching defects.[11b,40] Such defects may include surface silanol groups, oxygen-rich defects, residual organic matter,[39a] and carbonaceous inclusions in the aluminosilicate network.[39b]

Although the matrix absorption effects make the interpretation of the absorption spectrum complicated below 300 nm, the excitation spectrum emphasizes the lower-energy bands,

dx.doi.org/10.1021/jp309873y | J. Phys. Chem. C 2013, 117, 2966−2975

revealing a more structured line shape. Figure 9a presents the excitation spectrum of the Ir(III) complex in the $Si_{0.90}Al_{0.10}Na_{0.10}O_2$ matrix with the emitting excitation cutoff wavelength represented by the vertical dashed line at 350 nm. The spectrum is deconvoluted in Gaussian peaks centered at 358 (72.7%), 423 (26.8%), and 443 nm (0.5%). Similarly to the description of the complex in DCM (Figure 4a–c), parts b–d of Figure 9 bring a comparison of the experimental data with TDDFT-calculated transitions in the lower energy range ($\lambda >$ 330 nm), with the Ir(III) complex in the dielectric media with ε = 15.6 without counterion (Figure 9b), and with Cl^- (Figure 9c) or $[Al(OH)_4]^-$ as counterions (Figure 9d). Black bars denote the singlet transitions, blue bars triplet transitions, and red bars the experimentally observed transitions. The calculated transitions and their oscillator strengths are summarized in Table S13 of the Supporting Information. As expected, this region is highly populated with triplet states (Figure 9b–d). Following the argument that the most intense excitation peak, observed experimentally at 358 nm, possesses the highest singlet character among all transitions in this range, we can evaluate the accuracy of the calculation by comparing this transition with the wavelength of the most intense singlet transition calculated in this range. The calculations with no counterion and by using chloride as counterion present this transition blue-shifted by 15 and 23 nm with respect to the experimental value. Using $[Al(OH)_4]^-$ as counterion, the TDDFT results indeed match the experimental one most closely (with a blue-shift of only 4 nm). Regarding the two other experimental excitation bands at 423 and 443 nm, once again the calculation including $[Al(OH)_4]^-$ predicts singlet–triplet excitations that are closer to the experimental observations than the other two calculations. This mismatch is probably the minimum obtainable considering the level of theory and simplifications employed in these calculations. Better results could be achieved if the spin–orbit coupling were taken into account in the calculations, hence describing transitions between singlet and triplet states, which are known to occur with high probability in the presence of heavy atoms like Iridium.[17b]

4. CONCLUSIONS

In summary, we have introduced the design, synthesis, and characterization of a new optical material based on a sodium aluminosilicate mesoporous glass with active $(AlO_4)^-$ sites capable of immobilizing cationic Ir(III) complexes. The encapsulation of the complex molecules in the solid host is irreversible and can be realized at fairly high loading values (up to 2.5×10^{-2} mol/dm^3). Compared to diluted solutions of this complex in DCM, the excited state lifetimes of the solid materials are significantly longer, and the quantum yields are comparable, suggesting no significant molecular aggregation. The influence of the host–guest electrostatic interactions on the electronic structure of the Ir(III) complex was experimentally probed by spectroscopy and theoretically investigated by DFT and TDDFT calculations. The latter were done by taking into account the chemical environment of the Ir(III) complex by inclusion of both the counterion representing the active site of the matrix and the matrix's dielectric constant. This methodology provided further insights into how the excited states of the Ir(III) complex may be influenced by its chemical environment. The calculations reveal that at low dielectric constants ($\varepsilon \leq 20$), as observed in such matrices, the counterion has a strong influence on the energy and orbital composition of the excited states.

■ ASSOCIATED CONTENT

Supporting Information

^{27}Al and ^{23}Na TQ-MAS NMR spectra, ^{29}Si MAS NMR spectra, structural diagrams, table of distances and angles, absorption spectra, SEM images, table of fitting components and weighted means of the PL lifetimes, excitation and emission spectra, and lists of excited states. This material is available free of charge via the Internet at http://pubs.acs.org.

■ AUTHOR INFORMATION

Corresponding Author

*E-mail: andreasc@ifsc.usp.br.

Author Contributions

The manuscript was written through contributions of all authors. All authors have given approval to the final version of the manuscript.

Notes

The authors declare no competing financial interest.

■ ACKNOWLEDGMENTS

We acknowledge financial support from the Brazilian research funding agencies CNPq and FAPESP. The use of the computational facilities at the LCCA-Laboratory of Advanced Scientific Computation of the University of São Paulo is gratefully appreciated. We also thank Prof. L. De Cola (WWU Münster-Germany) for making her lab facilities readily available for the preparation of the Ir(III) complex and Prof. Dr. J-C. M'Peko (IFSC-USP) for his help in measuring the dielectric constants. The help of Dr. Waldir Avansi for providing the SEM images and Dr. Cauê R. de Oliveira for making readily available the microscope of the National Nanotechnology Laboratory for Agribusiness (LNNA), Embrapa, São Carlos, Brazil, are also greatly appreciated. J.M.F.-H. would like to acknowledge Fundación Séneca (Agencia Regional de Investigación, Región de Murcia) for a grant.

■ ABBREVIATIONS

dfptrBn , 1-benzyl-4-(2,4-difluorophenyl)-1*H*-1,2,3-triazole; dmbpy , 4,4′-dimethyl-2,2′-bipyridine

■ REFERENCES

(1) (a) Sessolo, M.; Bolink, H. J. *Adv. Mater.* **2011**, *23* (16), 1829. (b) King, S. M.; Al-Attar, H. A.; Evans, R. J.; Congreve, A.; Beeby, A.; Monkman, A. P. *Adv. Funct. Mater.* **2006**, *16* (8), 1043. (c) Ulbricht, C.; Beyer, B.; Friebe, C.; Winter, A.; Schubert, U. S. *Adv. Mater.* **2009**, *21* (44), 4418. (d) Tsuboyama, A.; Iwawaki, H.; Furugori, M.; Mukaide, T.; Kamatani, J.; Igawa, S.; Moriyama, T.; Miura, S.; Takiguchi, T.; Okada, S.; Hoshino, M.; Ueno, K. *J. Am. Chem. Soc.* **2003**, *125* (42), 12971. (e) Yang, C. H.; Yang, S. H.; Hsu, C. S. *Nanotechnology* **2009**, *20* (31), 315601. (f) Costa, R. D.; Monti, F.; Accorsi, G.; Barbieri, A.; Bolink, H. J.; Orti, E.; Armaroli, N. *Inorg. Chem.* **2011**, *50* (15), 7229.

(2) (a) Lowry, M. S.; Bernhard, S. *Chem.—Eur. J.* **2006**, *12* (31), 7970. (b) Dragonetti, C.; Falciola, L.; Mussini, P.; Righetto, S.; Roberto, D.; Ugo, R.; Valore, A.; De Angelis, F.; Fantacci, S.; Sgamellotti, A.; Ramon, M.; Muccini, M. *Inorg. Chem.* **2007**, *46* (21), 8533. (c) Yang, C. H.; Beltran, J.; Lemaur, V.; Cornil, J.; Hartmann, D.; Sarfert, W.; Fröhlich, R.; Bizzarri, C.; De Cola, L. *Inorg. Chem.* **2010**, *49* (21), 9891. (d) Lo, S. C.; Harding, R. E.; Shipley, C. P.; Stevenson, S. G.; Burn, P. L.; Samuel, I. D. W. *J. Am. Chem. Soc.* **2009**, *131* (46), 16681.

(3) (a) Baldo, M. A.; O'Brien, D. F.; You, Y.; Shoustikov, A.; Sibley, S.; Thompson, M. E.; Forrest, S. R. *Nature* **1998**, *395* (6698), 151. (b) Baldo, M. A.; Lamansky, S.; Burrows, P. E.; Thompson, M. E.; Forrest, S. R. *Appl. Phys. Lett.* **1999**, *75* (1), 4. (c) Chen, F. C.; Yang, Y.; Thompson, M. E.; Kido, J. *Appl. Phys. Lett.* **2002**, *80* (13), 2308.
(4) (a) Costa, R. D.; Orti, E.; Bolink, H. J.; Graber, S.; Housecroft, C. E.; Constable, E. C. *J. Am. Chem. Soc.* **2010**, *132* (17), 5978. (b) Costa, R. D.; Pertegas, A.; Orti, E.; Bolink, H. J. *Chem. Mater.* **2010**, *22* (4), 1288. (c) Mydlak, M.; Bizzarri, C.; Hartmann, D.; Sarfert, W.; Schmid, G.; De Cola, L. *Adv. Funct. Mater.* **2010**, *20* (11), 1812. (d) Costa, R. D.; Ortí, E.; Bolink, H. J.; Monti, F.; Accorsi, G.; Armaroli, N. *Angew. Chem., Int. Ed.* **2012**, *51*, 8178.
(5) (a) Li, M. J.; Jiao, P. C.; He, W. W.; Yi, C. Q.; Li, C. W.; Chen, X.; Chen, G. N.; Yang, M. S. *Eur. J. Inorg. Chem.* **2011**, *2*, 197. (b) Liu, X. M.; Xi, N.; Liu, S. J.; Ma, Y.; Yang, H. R.; Li, H. R.; He, J. H.; Zhao, Q.; Li, F. Y.; Huang, W. *J. Mater. Chem.* **2012**, *22* (16), 7894.
(6) (a) Yu, J. S.; Huang, J. A.; Lin, H.; Jiang, Y. D. *J. Appl. Phys.* **2010**, *108* (11), 113111. (b) Shinpuku, Y.; Inui, F.; Nakai, M.; Nakabayashi, Y. *J Photochem. Photobiol. A* **2011**, *222* (1), 203.
(7) (a) Richter, M. M. *Chem. Rev.* **2004**, *104* (6), 3003. (b) Kim, J. I.; Shin, I. S.; Kim, H.; Lee, J. K. *J. Am. Chem. Soc.* **2005**, *127* (6), 1614. (c) Miao, W. J. *Chem. Rev.* **2008**, *108* (7), 2506.
(8) (a) DiSalle, B. F.; Bernhard, S. *J. Am. Chem. Soc.* **2011**, *133* (31), 11819. (b) Mori, K.; Tottori, M.; Watanabe, K.; Che, M.; Yamashita, H. *J. Phys. Chem. C* **2011**, *115* (43), 21358.
(9) (a) Kawamura, Y.; Brooks, J.; Brown, J. J.; Sasabe, H. *Phys. Rev. Lett.* **2006**, *96* (1), 017404. (b) Lee, S. J.; Park, J. S.; Song, M.; Yoon, K. J.; Kim, Y. I.; Jin, S. H.; Seo, H. J. *Appl. Phys. Lett.* **2008**, *92* (19), 193312. (c) Waki, M.; Mizoshita, N.; Tani, T.; Inagaki, S. *Angew. Chem. Int. Ed.* **2011**, *50* (49), 11667.
(10) (a) Botelho, M. D. E. S.; Fernandez-Hernandez, J. M.; de Queiroz, T. B.; Eckert, H.; DeCola, L.; de Camargo, A. S. S. *J. Mater. Chem.* **2011**, *21* (24), 8829. (b) Aiello, D.; Talarico, A. M.; Teocoli, F.; Szerb, E. I.; Aiello, I.; Testa, F.; Ghedini, M. *New J. Chem.* **2011**, *35* (1), 141.
(11) (a) Kim, S. J.; Zhang, Y. D.; Zuniga, C.; Barlow, S.; Marder, S. R.; Kippelen, B. *Org. Electron.* **2011**, *12* (3), 492. (b) Rothe, C.; King, S.; Monkman, A. P. *Phys. Rev. B* **2006**, *73* (24), 245208.
(12) DiMarco, G.; Lanza, M.; Pieruccini, M.; Campagna, S. *Adv. Mater.* **1996**, *8* (7), 576.
(13) Goushi, K.; Kwong, R.; Brown, J. J.; Sasabe, H.; Adachi, C. *J. Appl. Phys.* **2004**, *95* (12), 7798.
(14) Jian, Y. A.; Peng, S. M.; Li, X. L.; Wen, X.; He, J. H.; Jiang, L.; Dang, Y. F. *Inorg. Chim. Acta* **2011**, *368* (1), 37.
(15) Deshpande, R. R.; Eckert, H. *J. Mater. Chem.* **2009**, *19* (21), 3419.
(16) Fernandez-Hernandez, J. M.; Yang, C. H.; Beltran, J. I.; Lemaur, V.; Polo, F.; Fröhlich, R.; Cornil, J.; De Cola, L. *J. Am. Chem. Soc.* **2011**, *133* (27), 10543.
(17) (a) Lee, S. C.; Ham, H. W.; Kim, Y. S. *J. Nanosci. Nanotechnol.* **2011**, *11* (5), 4557. (b) Smith, A. R. G.; Burn, P. L.; Powell, B. J. *ChemPhysChem* **2011**, *12* (13), 2428.
(18) (a) Asada, T.; Hamamura, S.; Matsushita, T.; Koseki, S. *Res. Chem. Intermed.* **2009**, *35* (8−9), 851. (b) De Angelis, F.; Fantacci, S.; Evans, N.; Klein, C.; Zakeeruddin, S. M.; Moser, J. E.; Kalyanasundaram, K.; Bolink, H. J.; Grätzel, M.; Nazeeruddin, M. K. *Inorg. Chem.* **2007**, *46* (15), 5989. (c) Minaev, B.; Minaeva, V.; Agren, H. *J. Phys. Chem. A* **2009**, *113* (4), 726.
(19) Dedeian, K.; Shi, J. M.; Forsythe, E.; Morton, D. C.; Zavalij, P. Y. *Inorg. Chem.* **2007**, *46* (5), 1603.
(20) (a) Medek, A.; Harwood, J. S.; Frydman, L. *J. Am. Chem. Soc.* **1995**, *117* (51), 12779. (b) Amoureux, J. P.; Fernandez, C.; Steuernagel, S. *J. Magn. Reson. Ser. A* **1996**, *123* (1), 116.
(21) Lee, S. K.; Stebbins, J. F. *Geochim. Cosmochim. Acta* **2003**, *67* (9), 1699.
(22) Brunauer, S.; Emmett, P. H.; Teller, E. *J. Am. Chem. Soc.* **1938**, *60*, 309.
(23) Barrett, E. P.; Joyner, L. G.; Halenda, P. P. *J. Am. Chem. Soc.* **1951**, *73* (1), 373.
(24) Kresge, C. T.; Leonowicz, M. E.; Roth, W. J.; Vartuli, J. C.; Beck, J. S. *Nature* **1992**, *359* (6397), 710.
(25) (a) Becke, A. D. *Phys. Rev. A* **1988**, *38* (6), 3098. (b) Becke, A. D. *J. Chem. Phys.* **1993**, *98* (7), 5648. (c) Lee, C. T.; Yang, W. T.; Parr, R. G. *Phys Rev B* **1988**, *37* (2), 785.
(26) (a) Perdew, J. P.; Burke, K.; Ernzerhof, M. *Phys. Rev. Lett.* **1996**, *77* (18), 3865. (b) Adamo, C.; Barone, V. *J. Chem. Phys.* **1999**, *110* (13), 6158.
(27) (a) Miertus, S.; Scrocco, E.; Tomasi, J. *Chem. Phys.* **1981**, *55* (1), 117. (b) Miertus, S.; Tomasi, J. *Chem. Phys.* **1982**, *65* (2), 239. (c) Pascualahuir, J. L.; Silla, E.; Tomasi, J.; Bonaccorsi, R. *J. Comput. Chem.* **1987**, *8* (6), 778. (d) Tomasi, J.; Mennucci, B.; Cammi, R. *Chem. Rev.* **2005**, *105* (8), 2999.
(28) Tamayo, A. B.; Garon, S.; Sajoto, T.; Djurovich, P. I.; Tsyba, I. M.; Bau, R.; Thompson, M. E. *Inorg. Chem.* **2005**, *44* (24), 8723.
(29) (a) Hay, P. J.; Wadt, W. R. *J. Chem. Phys.* **1985**, *82* (1), 299. (b) Hay, P. J.; Wadt, W. R. *J. Chem. Phys.* **1985**, *82* (1), 270.
(30) Clark, T.; Chandrasekhar, J.; Spitznagel, G. W.; Schleyer, P. V. *J. Comput. Chem.* **1983**, *4* (3), 294.
(31) (a) Petersson, G. A.; Allaham, M. A. *J. Chem. Phys.* **1991**, *94* (9), 6081. (b) Petersson, G. A.; Bennett, A.; Tensfeldt, T. G.; Allaham, M. A.; Shirley, W. A.; Mantzaris, J. *J. Chem. Phys.* **1988**, *89* (4), 2193.
(32) O'Boyle, N. M.; Tenderholt, A. L.; Langner, K. M. *J. Comput. Chem.* **2008**, *29* (5), 839.
(33) De Souza, J. E.; M'Peko, J. C.; Hernandes, A. C. *Appl. Phys. Lett.* **2007**, *91* (6), 064105.
(34) Sing, K. S. W.; Everett, D. H.; Haul, R. A. W.; Moscou, L.; Pierotti, R. A.; Rouquerol, J.; Siemieniewska, T. *Pure Appl. Chem.* **1985**, *57* (4), 603.
(35) Holzer, W.; Penzkofer, A.; Tsuboi, T. *Chem. Phys.* **2005**, *308* (1−2), 93.
(36) (a) Tamayo, A. B.; Alleyne, B. D.; Djurovich, P. I.; Lamansky, S.; Tsyba, I.; Ho, N. N.; Bau, R.; Thompson, M. E. *J. Am. Chem. Soc.* **2003**, *125* (24), 7377. (b) Bolink, H. J.; Coronado, E.; Costa, R. D.; Lardies, N.; Orti, E. *Inorg. Chem.* **2008**, *47* (20), 9149. (c) Bolink, H. J.; Cappelli, L.; Cheylan, S.; Coronado, E.; Costa, R. D.; Lardies, N.; Nazeeruddin, M. K.; Orti, E. *J. Mater. Chem.* **2007**, *17* (48), 5032. (d) Watts, R. J.; Missimer, D. *J. Am. Chem. Soc.* **1978**, *100* (17), 5350.
(37) Vlcek, A.; Zalis, S. *Coord. Chem. Rev.* **2007**, *251* (3−4), 258.
(38) (a) Siddique, Z. A.; Yamamoto, Y.; Ohno, T.; Nozaki, K. *Inorg. Chem.* **2003**, *42* (20), 6366. (b) Abedin-Siddique, Z.; Ohno, T.; Nozaki, K. *Inorg. Chem.* **2004**, *43* (2), 663.
(39) (a) Garcia, M. A.; Paje, S. E.; Villegas, M. A.; Llopis, J. *Mater. Lett.* **2000**, *43* (1−2), 23. (b) Green, W. H.; Le, K. P.; Grey, J.; Au, T. T.; Sailor, M. J. *Science* **1997**, *276* (5320), 1826.
(40) (a) Rothe, C.; Monkman, A. P. *Phys. Rev. B* **2003**, *68* (7), 075208. (b) Meskers, S. C. J.; Hubner, J.; Oestreich, M.; Bässler, H. *Chem. Phys. Lett.* **2001**, *339* (3−4), 223. (c) Richert, R.; Bässler, H. *Chem. Phys. Lett.* **1985**, *118* (3), 235. (d) Richert, R.; Bässler, H. *J. Chem. Phys.* **1986**, *84* (6), 3567.